Ultrasonics Sonochemistry 78 (2021) 105736

Contents lists available at ScienceDirect

Ultrasonics Sonochemistry

journal homepage: www.elsevier.com/locate/ultson

Numerical modeling of ultrasonic cavitation by dividing coated microbubbles into groups

Yanghui Ye [a], Yangyang Liang [b,*], Cong Dong [a], Zhongming Bu [a], Guoneng Li [a], Youqu Zheng [a]

[a] Department of Energy and Environment System Engineering, Zhejiang University of Science and Technology, Hangzhou 310023, China
[b] College of Mechanical Engineering, Zhejiang University of Technology, Hangzhou, China

ARTICLE INFO

Keywords:
Ultrasonic cavitation
Homogeneous model
Grouping
Coated microbubble

ABSTRACT

Homogeneous cavitation models usually use an average radius to predict the dynamics of all bubbles. However, bubbles with different sizes may have quite different dynamic characteristics. In this study, the bubbles are divided into several groups by size, and the volume-weighted average radius is used to separately calculate the dynamics of each group using a modified bubble dynamics equation. In the validation part, the oscillations of bubbles with two sizes are simulated by dividing them into 2 groups. Comparing with the predictions by the Volume of Fluid (VOF) method, the bubble dynamics of each size are precisely predicted by the proposed model. Then coated microbubbles with numerous sizes are divided into several groups in equal quantity, and the influence of the group number is analyzed. For bubble oscillations at $f = 0.1$ MHz and 1 MHz without ruptures, the oscillation amplitude is obviously under-estimated by the 1-group model, while they are close to each other after the group number increases to 9. For bubble ruptures triggered by Gaussian pulses, the predictions are close to each other when more than 5 groups are used.

1. Introduction

Ultrasonic cavitation can be utilized for ultrasonic imaging [1], stone fragmentation [2], drug delivery [3], gene transfection [4], cancer treatment [5], ultrasonic cleaning [6], water treatment [7], sonochemical fabrication [8] and so on [9]. Coated microbubbles have been widely applied in the biomedical ultrasonic diagnosis and treatment [10,11]. To improve the stability, coated microbubbles are made of high-molecular-weight inert gases and coated by lipid, protein or polymer shells. The characterization of coated microbubbles has been widely investigated by experimental [[12,13] and theoretical means [14,15]. In theoretical investigations, the Rayleigh-Plesset equation [16] provides the basis for the prediction of bubble dynamics; several models [17–20] have been proposed to consider the influence of the bubble shell; besides, the bubble–bubble interaction needs to be considered [21,22].

The numerical analysis is also widely used for the investigations of cavitation over the last two decades. Interface capturing methods such as VOF can precisely predict the bubble dynamics [23,24]. However, they are too expensive in the computational cost for the prediction of bubble clouds, since the bubbles are large in amount and numerous grids are needed to capture each bubble. Moreover, it is complex for interface capturing methods to model the bubble shell. Thus homogeneous models are usually used for the prediction of bubbly flows [25,26], which can greatly reduce the computational cost. Ye et al. [27,28] proposed a homogeneous cavitation model based on the bounded Rayleigh-Plesset equation, and this dynamic equation was modified in their study due to the homogeneous treatment. In this model, the compressibility of the liquid was considered while the density of the gas was set to constant, since the growth/collapse of bubbles have been considered by the add/remove of vapor. For the same reason, there is no need to consider the bubble–bubble interaction for the numerical analysis. This cavitation model can precisely predict the dynamics of the equal-sized spherical bubbles in stationary liquid.

The initial radius (R_0) distributes in a wide range for both natural and artificial cavitation bubbles. Gorce et al. [29] carried out theoretical calculations to investigate the influence of bubble size on the echogenicity of microbubbles. In their calculations, coated microbubbles were divided into five groups with equal numbers. It was found that bubbles with $R_0 < 1$ μm accounted for 60% of the number but did not contribute appreciably to the echogenicity, this is why the bubble volume appears to be a much better indicator of echogenicity than the bubble count. Haghi et al. [15] also conducted theoretical investigations on the

* Corresponding author.
E-mail address: liangyy@zjut.edu.cn (Y. Liang).

https://doi.org/10.1016/j.ultsonch.2021.105736
Received 21 June 2021; Received in revised form 13 August 2021; Accepted 21 August 2021
Available online 26 August 2021

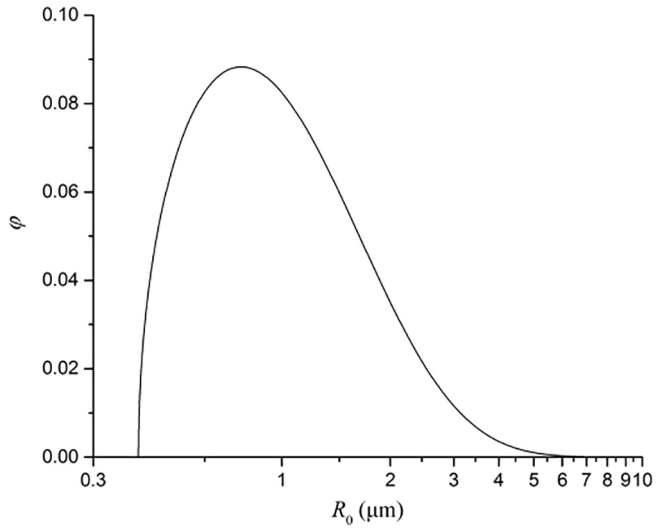

Fig. 1. The dimensionless bubble number density distribution fitted from the data in Ref. [29].

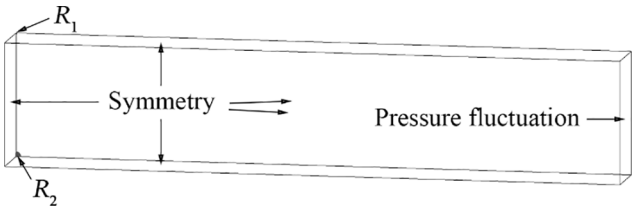

Fig. 2. Computational domain and boundary conditions for the cases of microbubbles with two sizes.

Table 1
Bubble radii for the validation cases with two bubble sizes. The volume-weighted average radius is used for the traditional homogeneous model.

Case	R_{10}/μm	R_{20}/μm	$\overline{R}$/μm
A	1	2	1.6510
B	1	4	3.1913
C	1	8	6.3537

interactions of microbubbles with different sizes. It was found that the dynamics of the cluster was dominated by the largest microbubbles, and they even in small numbers can force smaller bubbles into period doubling and subharmonic oscillations. Thus different bubbles may have quite different dynamic characteristics.

In numerical homogeneous models, an average R_0 is usually used, which means the differences of the bubble dynamics with different R_0 are neglected and the complex inter-bubble interactions can not be predicted. In this study, the microbubbles are divided into several groups by R_0 in equal quantity, and the bubble dynamics equation is modified accordingly; the volume-weighted average R_0 is used to calculate the bubble dynamics of each group separately. In the validation part, we firstly exam the ability of the proposed model for the prediction of bubble dynamics with several sizes: the oscillations of bubbles with two sizes are simulated by dividing them into 2 groups, and comparisons with the predictions by the VOF method are made. Then coated microbubbles with numerous sizes are divided into groups, and the influence of the group number on their oscillations and ruptures are analyzed.

2. Mathematical model

2.1. Grouping of coated microbubbles

The average R_0 of coated microbubbles is usually around 1 μm. In this study, the dimensionless bubble number density distribution is described by:

$$\varphi = e^{-(R_0-0.4)/0.75}\sqrt{1-e^{-(R_0-0.4)/17.5}}\ (0.4\ \mu\mathrm{m}\leqslant R_0\leqslant 10\mu\mathrm{m}) \tag{1}$$

which is fitted from the data for SonoVue® microbubbles in Ref. [29] and shown in Fig. 1. This function is replaceable for other microbubbles. The microbubbles are divided into i groups in equal quantity, the size range of group j can be obtained by solving the integral upper limit of the following equation:

$$\int_{R_{j,L}}^{R_{j,U}} \varphi dR_0 = \frac{1}{i}\int_{0.4\mu m}^{10\mu m} \varphi dR_0 \tag{2}$$

where j is from 1 to i-1, the integral lower limit of the first group $R_{1,\mathrm{L}} =$ 0.4 μm and $R_{j+1,\mathrm{L}} = R_{j,\mathrm{U}}$. After obtaining the range of each group, the initial volume-weighted average radius of group j can be obtained by:

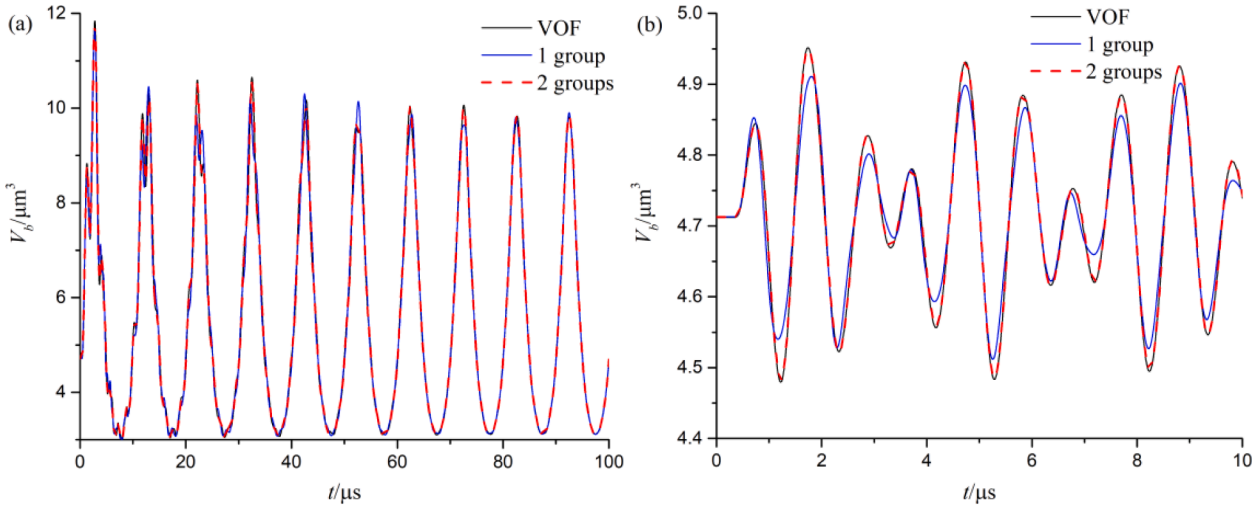

Fig. 3. Evolutions of V_b of Case A predicted by the VOF method and the homogeneous models with 1 group (traditional model) and 2 groups (proposed model) at (a) $f = 0.1$ MHz, $A_p = 0.5$ and (b) $f = 1$ MHz, $A_p = 0.01$. The surface tension is neglected.

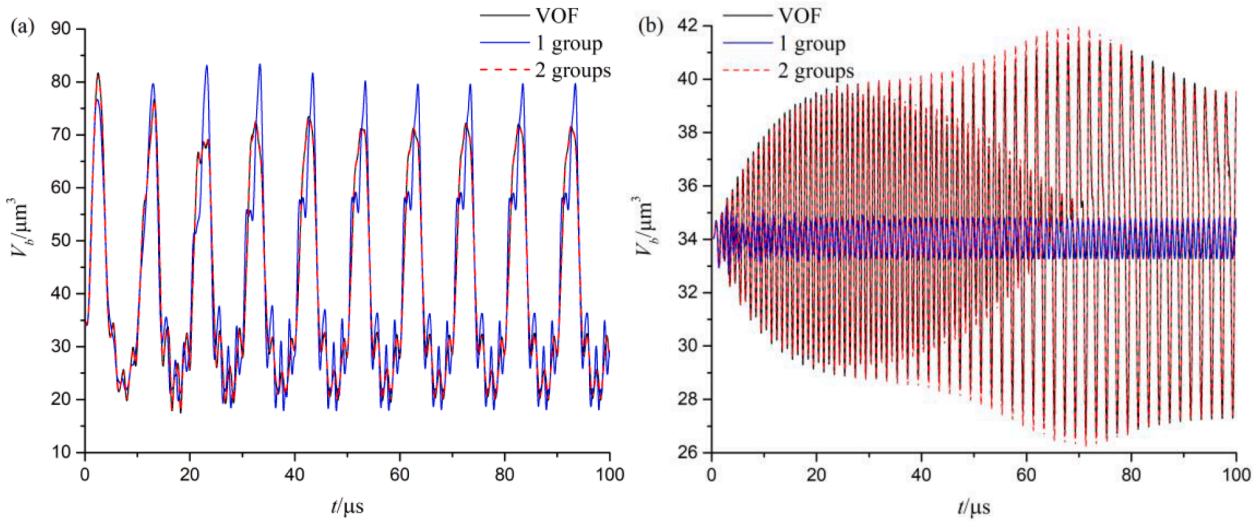

Fig. 4. Evolutions of V_b of Case B predicted by the VOF method and the homogeneous models with 1 group and 2 groups at (a) $f = 0.1$ MHz, $A_p = 0.5$ and (b) $f = 1$ MHz, $A_p = 0.01$. The surface tension is neglected.

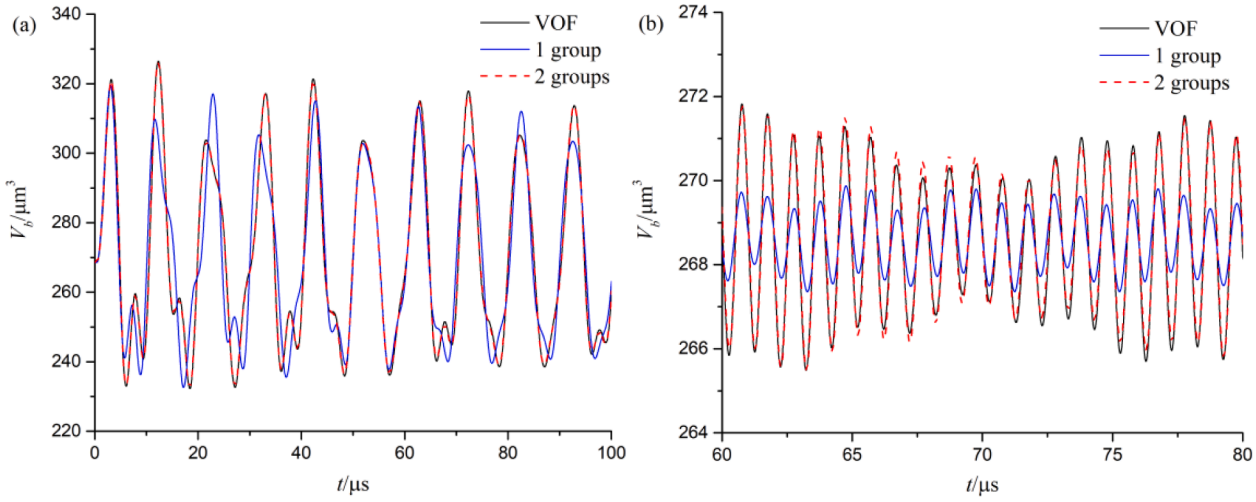

Fig. 5. Evolutions of V_b of Case C predicted by the VOF method and the homogeneous models with 1 group and 2 groups at (a) $f = 0.1$ MHz, $A_p = 0.1$ and (b) $f = 1$ MHz, $A_p = 0.01$. The surface tension is neglected.

$$R_{j0} = \sqrt[3]{\frac{\int_{R_{j,\mathrm{L}}}^{R_{j,\mathrm{U}}} \varphi R_0^3 dR_0}{\int_{R_{j,\mathrm{L}}}^{R_{j,\mathrm{U}}} \varphi dR_0}} \tag{3}$$

And the initial gas volume fraction of group j is obtained as:

$$\alpha_{j0} = \frac{4\pi}{3}\frac{n_0}{i}R_{j0}^3 \tag{4}$$

where n_0 denotes the initial bubble number density.

2.2. Homogeneous cavitation model

Homogeneous cavitation models usually use the average bubble radius to predict the dynamics of all bubbles. In this study, the micro-bubbles are divided into several groups, and the volume-weighted average radius is used to predict the bubble dynamics of each group. Traditional homogeneous cavitation models usually have 2 phases: the liquid phase and the gas phase. This new homogeneous cavitation model includes $1 + i$ phases, with one representing the liquid and the others representing each group. The dynamics of 3D bubbles are calculated by the Ye's equal-sized cavitation model [27] with several modifications.

Since the bubbles are divided into i groups, the bubble radius of group j is modified to:

$$R_j = \sqrt[3]{\frac{3i}{4\pi n}\alpha_j} \tag{5}$$

where n is the bubble number density. In Ye's model [27], the local pressure p was supposed to be equal to the pressure at the boundary of the region occupied by the bubble, and the equivalent radius of this region was denoted by R_e. For the bubbles with different sizes, we suppose that the region occupied by a bubble is proportional to the volume of this bubble, then R_{ej} is modified to:

$$\frac{4\pi}{3}\frac{n}{i}R_{ej}^3 = 1\cdot\frac{\alpha_j}{1-\alpha_L} \tag{6}$$

where α_L is the liquid volume fraction. Thus the relationship between R_j and R_{ej} is modified to:

$$\frac{R_j^3}{R_{ej}^3} = 1 - \alpha_L \tag{7}$$

Then the bubble dynamics equation in Ye's model [27] is modified

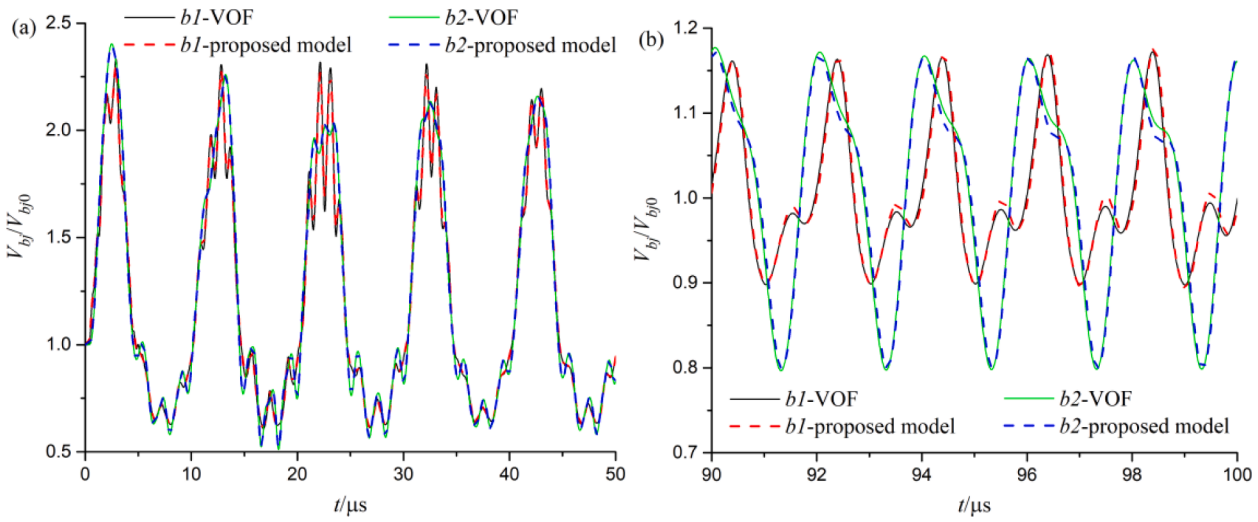

Fig. 6. Evolutions of relative V_{bj} (bubble volume of group j) of Case B predicted by the VOF method and the proposed model at (a) $f = 0.1$ MHz, $A_p = 0.5$ and (b) $f = 1$ MHz, $A_p = 0.01$.

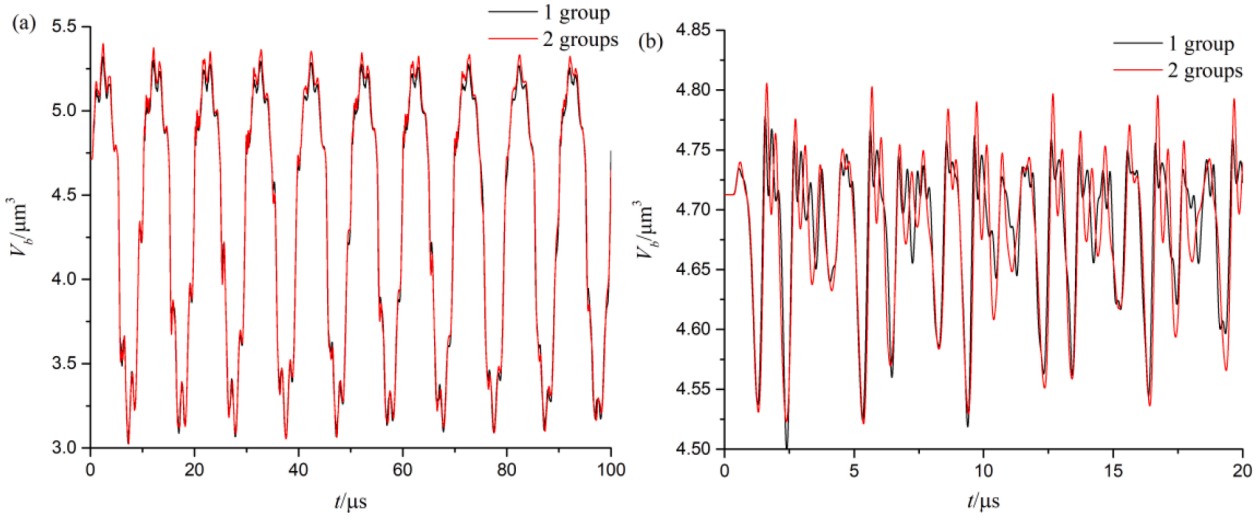

Fig. 7. Evolutions of V_b of Case A predicted by the homogeneous models with 1 group and 2 groups at (a) $f = 0.1$ MHz, $A_p = 0.5$ and (b) $f = 1$ MHz, $A_p = 0.01$. The shell properties are considered by the Marmottant model [19].

to:

$$\ddot{R}_j = \frac{p_{bj} - p/\rho_L + \left(0.4(1-\alpha_L)^{7/3} - 1.3(1-\alpha_L)^{4/3} + 2.4(1-\alpha_L)^{1/3} - 1.5\right)\dot{R}_j^2}{\left(1 + 0.2(1-\alpha_L)^{4/3} - 1.2(1-\alpha_L)^{1/3}\right)R_j} \tag{8}$$

where p_{bj} is the liquid pressure at the bubble surface of group j and ρ_L is the liquid density. As in Ref. [27], a minimum collapse rate is given, below which the collapse rate will not decrease any more. For free spherical bubbles without the shell, suppose the gas inside bubbles is a uniform (both in content and temperature) perfect gas and no diffusion of non-condensable gas in the liquid, p_{bj} can be obtained as [30]:

$$p_{bj} = p_{Vj} + \left(p_0 + \frac{2\sigma_L}{R_{j0}} - p_s\right)\left(\frac{R_{j0}}{R_j}\right)^{3\gamma} - \frac{2\sigma_L}{R_j} - \frac{4\mu_L\dot{R}_j}{R_j} \tag{9}$$

where p_{Vj} is the partial pressure of vapor, p_0 is the initial pressure outside the bubble, σ_L is the surface tension coefficient, p_s is the saturated vapor pressure, γ is the polytropic index and μ_L is the dynamic viscosity of liquid. For coated microbubbles, the Marmottant model [19] is used to model the shell in this study. Supposing the buckling radius equals to R_{j0}, p_{bj} is obtained as [19]:

$$p_{bj} = p_{Vj} + \left(p_0 + \frac{2\sigma(R_{j0})}{R_{j0}} - p_s\right)\left(\frac{R_{j0}}{R_j}\right)^{3\gamma} - \frac{2\sigma(R_j)}{R_j} - \left(\mu_L + \frac{\kappa_s}{R_j}\right)\frac{4\dot{R}_j}{R_j} \tag{10}$$

$$\sigma(R_j) = \begin{cases} \chi\left(max\left(\frac{R_j}{R_{j0}}, 1\right)^2 - 1\right) & \mathrm{R_j} \leqslant \mathrm{R_{ruptured}} \\ \sigma_L & \mathrm{R_j} > \mathrm{R_{ruptured}} \end{cases} \tag{11}$$

where the shell viscosity $\kappa_s = 1.5 \times 10^{-9}$ kg/s, the elastic modulus $\chi = 0.5$ N/m [31] and the rupture radius $R_{\mathrm{ruptured}} = 1.5R_{j0}$ [20] in this study.

n_0 is recorded by a transport equation [27]:

$$\frac{\partial(\rho_L\alpha_L n_0)}{\partial t} + \nabla(\rho_L\alpha_L n_0 \boldsymbol{V}) = 0 \tag{12}$$

Then n can be obtained as:

$$n = \frac{n_0\alpha_L}{\alpha_{L0}} \tag{13}$$

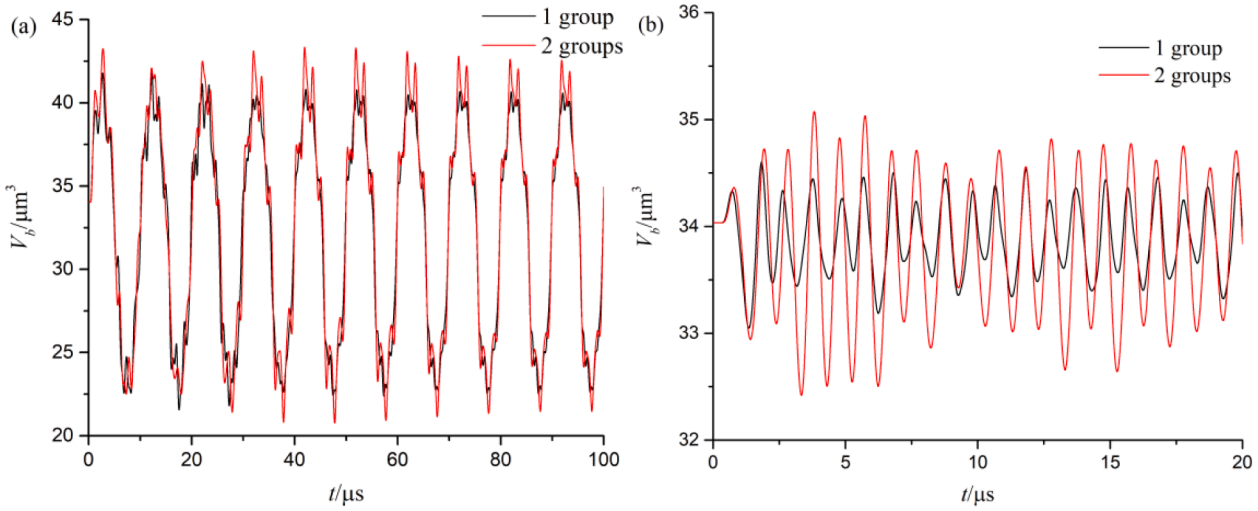

Fig. 8. Evolutions of V_b of Case B predicted by the homogeneous models with 1 group and 2 groups at (a) $f = 0.1$ MHz, $A_p = 0.5$ and (b) $f = 1$ MHz, $A_p = 0.01$. The shell properties are considered by the Marmottant model [19].

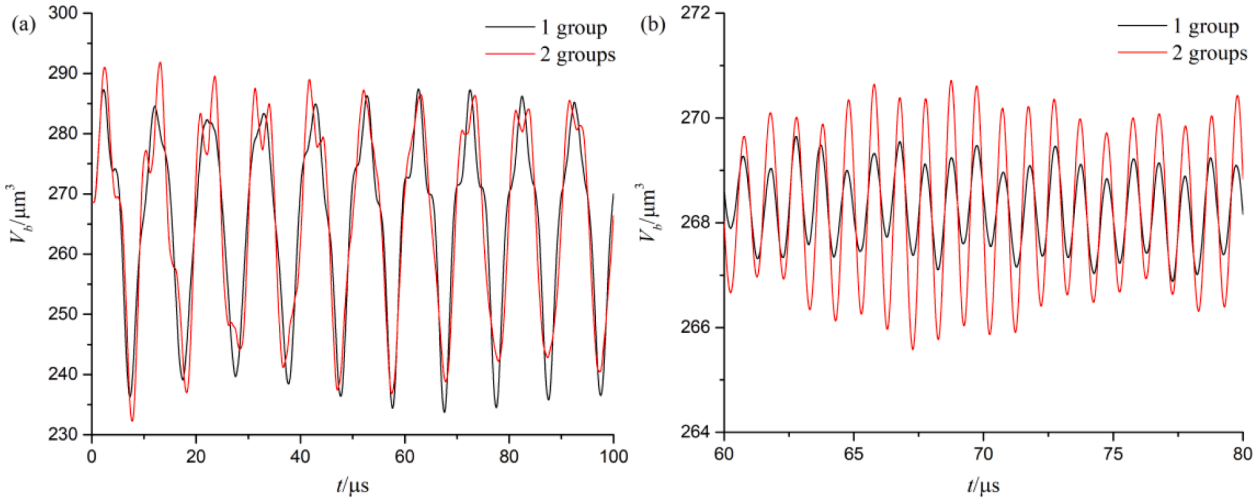

Fig. 9. Evolutions of V_b of Case C predicted by the homogeneous models with 1 group and 2 groups at (a) $f = 0.1$ MHz, $A_p = 0.1$ and (b) $f = 1$ MHz, $A_p = 0.01$. The shell properties are considered by the Marmottant model [19].

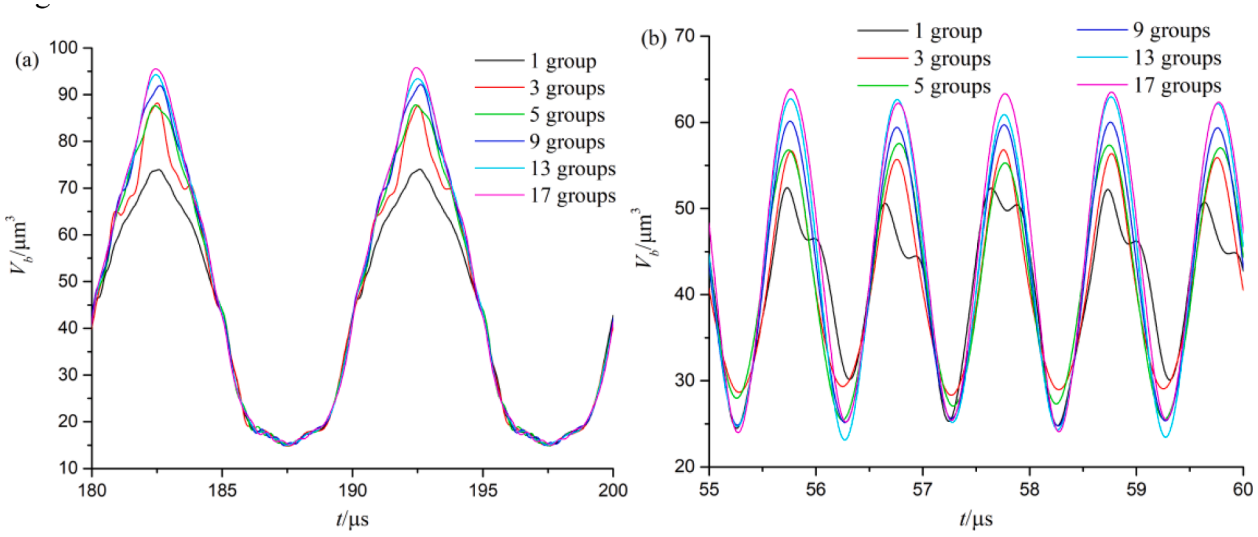

Fig. 10. Evolutions of V_b predicted by the homogeneous models with different i at (a) $f = 0.1$ MHz, $A_p = 2$ and (b) $f = 1$ MHz, $A_p = 0.5$. No bubble rupture occurs.

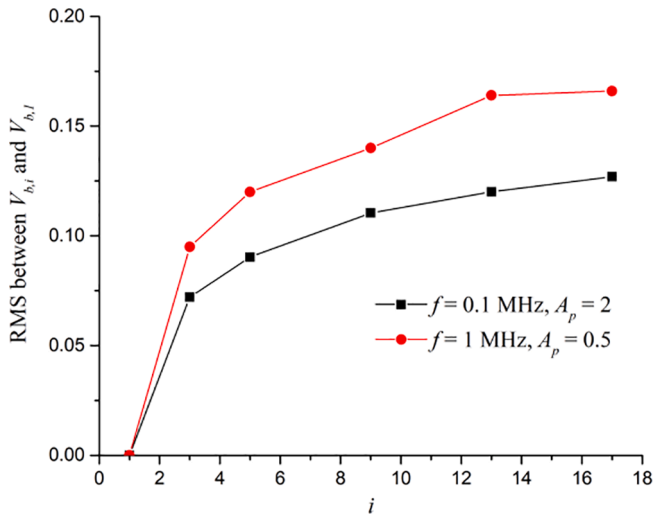

Fig. 11. Root mean square of the relative differences between V_b predicted by the i-groups model ($V_{b,i}$) and 1-group model ($V_{b,1}$) at $f = 0.1$ MHz and 1 MHz.

where α_{L0} is the initial liquid volume fraction. Another i transport equations are added to respectively record $\dot{R}_j$. Finally, the change rate of the gas volume fraction of group j can be obtained as:

$$\frac{d\alpha_j}{dt} = \frac{4\pi n}{i} R_j^2 \dot{R}_j \tag{14}$$

The compressibility of liquid is modeled by the Tait's equation of state for water [32,33]:

$$\left(\frac{\rho_L}{\rho_{L0}}\right)^m = 1 + \frac{m(p - p_0)}{K_0} \tag{15}$$

where $\rho_{L0} = 1000$ kg/m^3, $m = 7.15$ and $K_0 = 2.2 \times 10^9$ Pa. The gas density is the same for all groups and set to be constant.

2.3. Validation

A sine pressure wave and a Gaussian pulse in the following forms are respectively employed:

$$p = p_0\left(1 - A_p \cdot sin(2\pi ft)\right) \tag{16}$$

$$p = p_0\left(1 - A_p \cdot e^{-(t/t_w - 3)^2}\right) \tag{17}$$

where t denotes time and A_p denotes the amplitude of the pressure fluctuation. The sine wave is used to produce the bubble oscillation and the Gaussian pulse is used to produce the bubble rupture. The simulation time-step sizes are respectively $1/500f$ and $t_w/500$. Firstly, cases with two bubble sizes are simulated in Section 3.1, and comparisons are made with those predicted by the VOF method. Then cases with numerous coated microbubbles are simulated in Sections 3.2 and 3.3 to analyze the influence of the group number. All flows in the validation part are considered to be laminar and $p_0 = 0.1$ MPa, $\mu_L = 0.001$ Pa·s. The gravity and phase change are neglected.

3. Results and discussion

3.1. Microbubbles with two sizes

The dynamics of two bubbles inside a rectangular tube are simulated as shown in Fig. 2. The computational domain is 0.1 mm in height, 0.5 mm in length and 0.05 mm in width. A sine pressure wave is specified at the right face while the other five are symmetry planes. Two bubbles with initial radii of R_{10} and R_{20} are located at the left corner, one in the upper corner and the other in the lower corner, which means only one eighth of each bubble is inside the computational domain and the bubble distance is 0.1 mm. Firstly, cases as shown in Table 1 are simulated by the VOF method and homogeneous models. In order to reduce the deviations caused by the estimations of the pressure inside bubbles, the flow is assumed to be isothermal ($\gamma = 1$) and the phase change is neglected ($p_V = 0$). Moreover, the surface tension is neglected ($\sigma_L = 0$) to simplify the calculation of the VOF method as in Ref. [27]. After that, the shell properties are considered using the Marmottant model [19]. For the VOF method, 0.6 million tetrahedral meshes are employed and most of them concentrate around bubbles. More grids are needed if the bubble distance is increased, thus a small distance (0.1 mm) is used. For the homogeneous models, these cases are simplified as a 1D problem and 300 meshes are employed, and the bubbles distribute uniformly inside the region within 0.05 mm from the left boundary. For the proposed homogeneous model, the bubbles are divided into two groups whose initial radii are respectively R_{10} and R_{20}, and the initial bubble number density of each group is 5×10^{11} m^{-3}. The traditional homogeneous model which has only 1 group is also used for comparison, whose initial radius equals to the volume-weight average of R_{10} and R_{20}, and $n_0 = 10^{12}$ m^{-3}.

Figs. 3–5 show the evolutions of the total bubble volume (V_b) predicted by the VOF method and the homogeneous models with the group number $i = 1$ and 2 at $f = 0.1$ MHz and 1 MHz. It can be seen that the

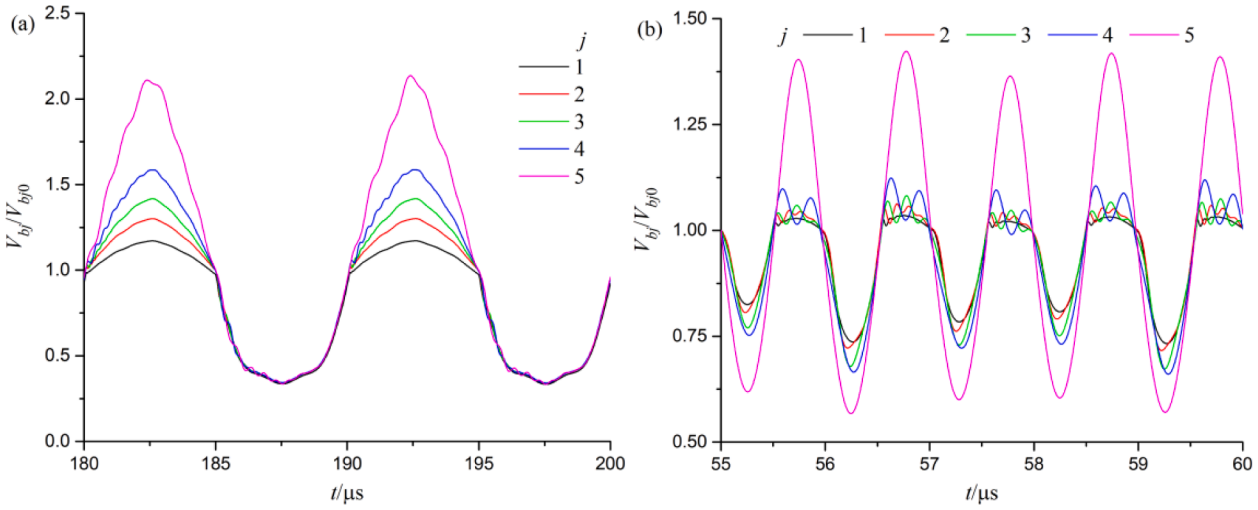

Fig. 12. Evolutions of V_{bj} predicted by the homogeneous model with 5 groups at (a) $f = 0.1$ MHz, $A_p = 2$ and (b) $f = 1$ MHz, $A_p = 0.5$.

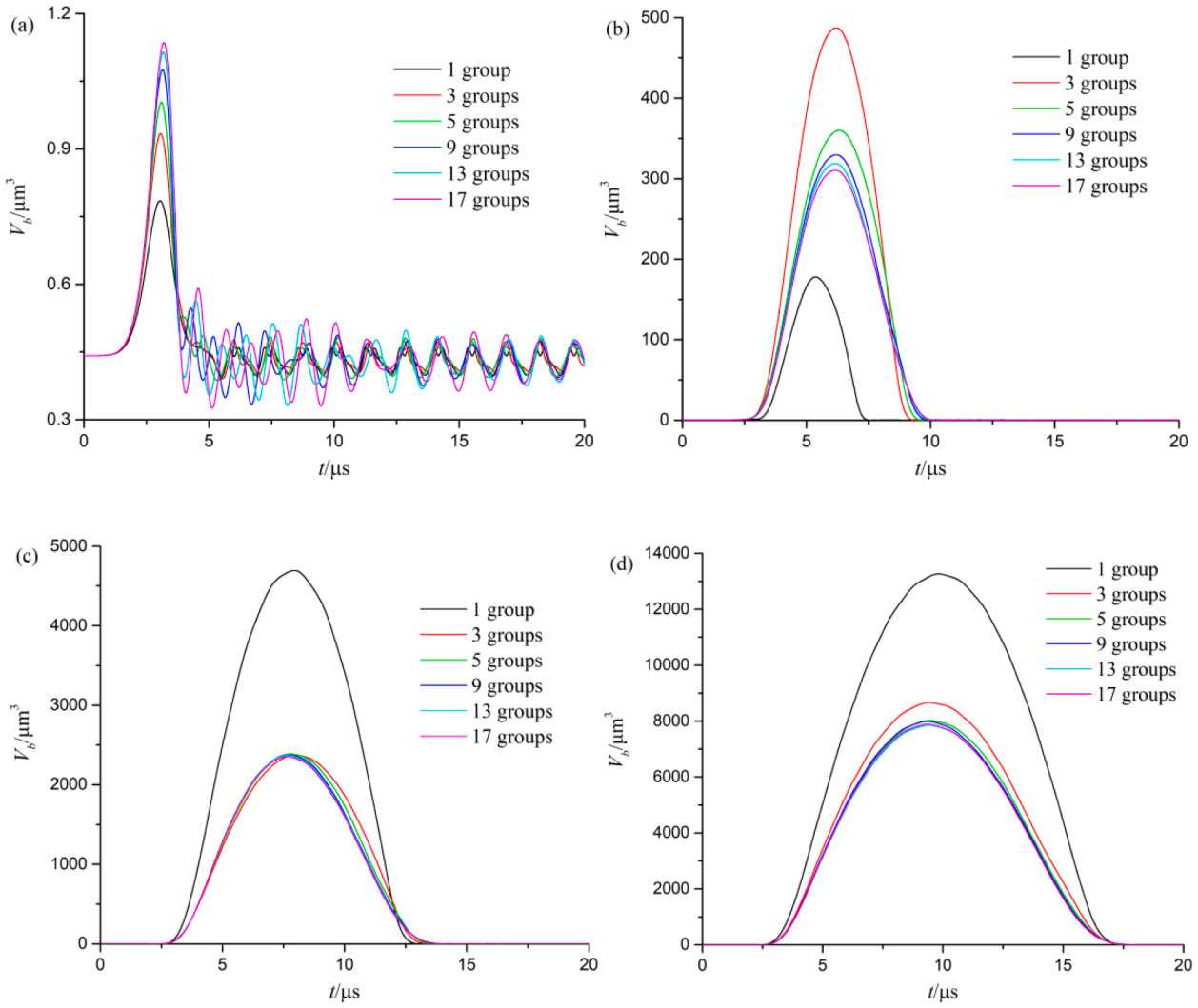

Fig. 13. Evolutions of V_b predicted by the homogeneous models with different i at $t_w = 1$ μs and $A_p =$ (a) 2, (b) 4, (c) 6, (d) 8. Bubble rupture occurs when $A_p = 4$, 6 and 8.

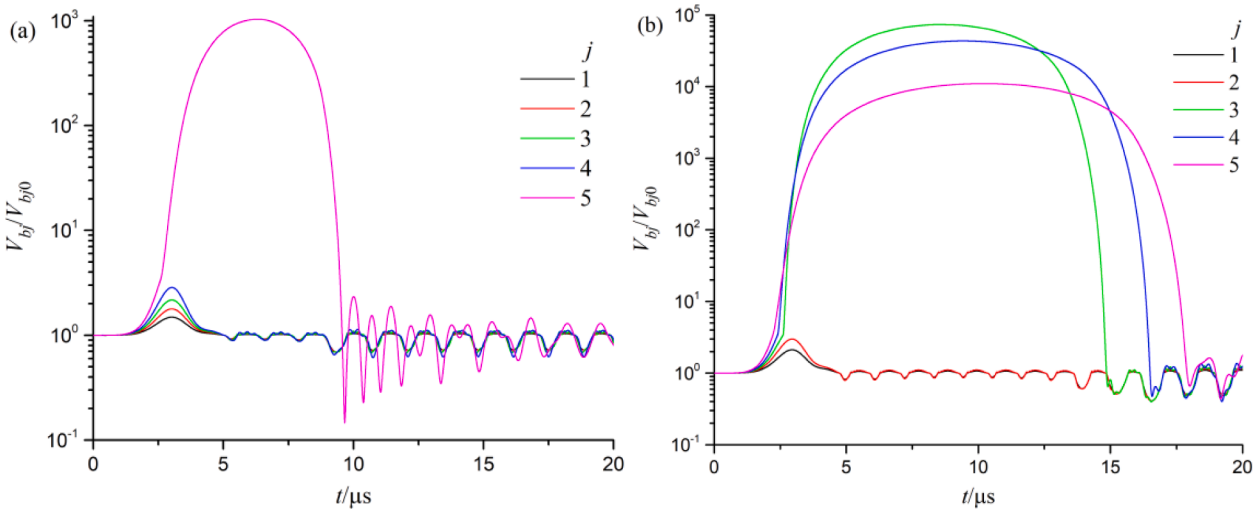

Fig. 14. Evolutions of V_{bj} predicted by the homogeneous model with 5 groups at $t_w = 1$ μs and $A_p =$ (a) 4, (b) 8.

bubble oscillations predicted by the VOF method and the proposed model match precisely with each other, while the differences are obvious from the predictions by the traditional homogeneous model, especially when the difference between R_{10} and R_{20} is large. Moreover, the oscillations of each bubble are also precisely predicted by the proposed model. Take Case B for example, Fig. 6 shows the evolutions of the relative bubble volume of each group (V_{bj}) at $f = 0.1$ MHz and 1 MHz, the dynamics of each group predicted by the proposed model also match well with that by the VOF method.

Then the shell properties are considered using the Marmottant model [19] ($\chi = 1.07$ and $\sigma_L = 0.072$ N/m). Since it is difficult for the VOF method to consider the influence of the bubble shell, only the predictions by the homogeneous models are compared. Figs. 7–9 show the evolutions of V_b predicted by the homogeneous models with $i = 1$ and 2 corresponding to the calculation conditions of Figs. 3–5. As expected, the fluctuation amplitude of V_b decreases after considering the surface tension, and the predictions by these two homogeneous models become closer to each other. Besides, the compression-only behavior [19] appears.

3.2. Coated microbubbles without rupture

For numerous coated microbubbles with different sizes, the grouping method described in Section 2.1 is used. The computational domain and boundary conditions shown in Fig. 2 are still used. Initially, the microbubbles occupy the left half part of the computational domain and $n_0 = 10^{12}$ m^{-3}. Fig. 10 shows the evolutions of V_b predicted by the homogeneous models with different i at $f = 0.1$ MHz and 1 MHz. At $f = 0.1$ MHz and $A_p = 2$ (further increase of A_p may lead to the bubble rupture), the maximum V_b increases obviously when i increases from 1 to 3, and it increases slightly when i increases from 13 to 17, while the bubble compression is almost independent on i. At $f = 1$ MHz and $A_p = 0.5$, the predictions of $i = 13$ and 17 are also close to each other. In order to exhibit the differences between these results more visually, Fig. 11 shows the root mean square (RMS) of the relative differences between V_b predicted by the i-groups model ($V_{b,i}$) and 1-group model ($V_{b,1}$) at each time step. It can be seen that the increase of RMS is small when i is larger than 9. Fig. 12 shows V_{bj} predicted by the homogeneous model with $i = 5$ corresponding to Fig. 10. At $f = 0.1$ MHz and $A_p = 2$, the bubble compressions of all groups are close, but during the bubble growth, the bubble volume increased by more than 110% for the largest group while it only increased by 17% for the smallest group. The growth of small bubbles are also obviously suppressed at $f = 1$ MHz. As concluded in previous researches [15,29,34], the oscillations of small bubbles are suppressed by large bubbles.

3.3. Coated microbubbles with rupture

The numerical settings are the same as that in Section 3.2 except that the sine wave is replaced by the Gaussian pulse to cause the bubble rupture, and $n_0 = 10^{10}$ m^{-3}. Since the Rayleigh-Plesset equation is applicable for spherical bubbles, a much smaller n_0 is used in this Section to prevent bubbles lose spherical shape after being close to each other. Fig. 13 shows the evolutions of V_b predicted by the homogeneous models with different i under different A_p. At $A_p = 2$, no bubble rupture occurs, and the maximum V_b increases with i as the cases above. At $A_p = 4$, the maximum V_b is under-estimated when $i = 1$, and it decreases with increasing i when $i \geq 3$. At $A_p = 6$ and 8, V_b is obviously over-predicted when $i = 1$, and the predictions are close to each other when $i \geq 5$. Fig. 14 shows the corresponding V_{bj} predicted by the homogeneous model with $i = 5$ at $A_p = 4$ and 8. At $A_p = 4$, R increases by 10 times for the largest group, while it does not reach R_{ruptured} for the other groups (Fig. 14 a), thus the bubble rupture only occurs to the largest group, which is 20% of the total bubbles. In addition, the bubble rupture occurs to one third of bubbles when $i = 3$ and around 23% of bubbles when $i = 9$, 13, 17. At $A_p = 8$, the bubble rupture occurs to the largest 3 groups, and the maximum V_{bj}/V_{bj0} decreases with increasing j in these 3 largest groups (Fig. 14 b).

4. Conclusions

Since the dynamics of bubbles with different initial sizes may be quite different, a new homogeneous cavitation model was proposed. In this model, bubbles are divided into groups by initial size, and the dynamics of each group are separately calculated using a modified bubble dynamics equation. According to the comparisons with the predictions by the VOF method, the dynamics of spherical bubbles with two sizes can be accurately predicted by calculating the bubble dynamics of each size separately. We believe that the bubble dynamics can still be well predicted by the proposed model when there are dozens of sizes. For coated microbubbles with numerous sizes, the influences of the group number on the predictions of bubble oscillations and ruptures were analyzed. For bubble oscillations at $f = 0.1$ MHz and 1 MHz, the bubble growths are obviously under-estimated when only 1 group is used, while they are close to each other after the group number increases to 9, and the group number has little influence on the bubble compression. During an oscillation, the amplitude of a group is smaller than that of a larger group, and the bubble growth of the smallest group is greatly suppressed due to the inter-bubble interactions. For bubble ruptures triggered by Gaussian pulses, the bubble growth predicted by the 1-group model is firstly under-estimated and then over-predicted with the increase of the pulse amplitude, and the predictions are close to each other when more than 5 groups are used.

CRediT authorship contribution statement

Yanghui Ye: Conceptualization, Methodology, Software. **Yangyang Liang:** Validation, Writing – original draft. **Cong Dong:** Investigation. **Zhongming Bu:** Visualization. **Guoneng Li:** Resources. **Youqu Zheng:** Supervision.

Declaration of Competing Interest

The authors declare that they have no known competing financial interests or personal relationships that could have appeared to influence the work reported in this paper.

Acknowledgments

Financial support from the Zhejiang Provincial Natural Science Foundation of China (No. LQ21E060003, LZ21E060001, LQ19E080002), National Natural Science Foundation of China (No. 51606169), Key R&D Plan of Zhejiang Province (No. 2020C03115) and Fundamental Research Funds of Zhejiang University of Science and Technology (No. 2021QN029).

Appendix A. Supplementary data

Supplementary data to this article can be found online at https://doi.org/10.1016/j.ultsonch.2021.105736.

References

[1] S. Qin, C.F. Caskey, K.W. Ferrara, Ultrasound contrast microbubbles in imaging and therapy: physical principles and engineering, Phys. Med. Biol. 54 (6) (2009) R27–R57.
[2] M. Basulto-Martínez, I. Klein, J. Gutiérrez-Aceves, The role of extracorporeal shock wave lithotripsy in the future of stone management, Curr. Opin. Urol. 29 (2) (2019) 96–102.
[3] Y. Yang, Q. Li, X. Guo, J. Tu, D. Zhang, Mechanisms underlying sonoporation: Interaction between microbubbles and cells, Ultrason. Sonochem. 67 (2020) 105096, https://doi.org/10.1016/j.ultsonch.2020.105096.
[4] B. Wu, Q. Qiao, X. Han, H. Jing, H. Zhang, H. Liang, W. Cheng, Targeted nanobubbles in low-frequency ultrasound-mediated gene transfection and growth

inhibition of hepatocellular carcinoma cells, Tumor Biology 37 (9) (2016) 12113–12121.
[5] A.K.W. Wood, C.M. Sehgal, A review of low-intensity ultrasound for cancer therapy, Ultrasound Med. Biol. 41 (4) (2015) 905–928.
[6] F. Reuter, R. Mettin, Mechanisms of single bubble cleaning, Ultrason. Sonochem. 29 (2016) 550–562.
[7] S. Anandan, V. Kumar Ponnusamy, M. Ashokkumar, A review on hybrid techniques for the degradation of organic pollutants in aqueous environment, Ultrason. Sonochem. 67 (2020) 105130, https://doi.org/10.1016/j.ultsonch.2020.105130.
[8] Z. Li, T. Zhuang, J. Dong, L. Wang, J. Xia, H. Wang, X. Cui, Z. Wang, Sonochemical fabrication of inorganic nanoparticles for applications in catalysis, Ultrason. Sonochem. 71 (2021) 105384, https://doi.org/10.1016/j.ultsonch.2020.105384.
[9] Y.e. Yao, Y. Pan, S. Liu, Power ultrasound and its applications: a state-of-the-art review, Ultrason. Sonochem. 62 (2020) 104722, https://doi.org/10.1016/j.ultsonch.2019.104722.
[10] C.E. Brennen, Cavitation in medicine, Interface Focus 5 (5) (2015) 20150022, https://doi.org/10.1098/rsfs.2015.0022.
[11] H. Mulvana, R.J. Browning, Y. Luan, N. de Jong, M.-X. Tang, R.J. Eckersley, E. Stride, Characterization of contrast agent microbubbles for ultrasound imaging and therapy research, IEEE Trans. Ultrason. Ferroelectr. Freq. Control 64 (1) (2017) 232–251.
[12] K.L. Tan, S.H. Yeo, Bubble dynamics and cavitation intensity in milli-scale channels under an ultrasonic horn, Ultrason. Sonochem. 58 (2019) 104666, https://doi.org/10.1016/j.ultsonch.2019.104666.
[13] L. Yusuf, M.D. Symes, P. Prentice, Characterising the cavitation activity generated by an ultrasonic horn at varying tip-vibration amplitudes, Ultrason. Sonochem. 70 (2021) 105273, https://doi.org/10.1016/j.ultsonch.2020.105273.
[14] L. Jiang, H. Ge, F. Liu, D. Chen, Investigations on dynamics of interacting cavitation bubbles in strong acoustic fields, Ultrason. Sonochem. 34 (2017) 90–97.
[15] H. Haghi, A.J. Sojahrood, M.C. Kolios, Collective nonlinear behavior of interacting polydisperse microbubble clusters, Ultrason. Sonochem. 58 (2019) 104708, https://doi.org/10.1016/j.ultsonch.2019.104708.
[16] M.S. Plesset, A. Prosperetti, Bubble dynamics and cavitation, Annu. Rev. Fluid Mech. 9 (1) (1977) 145–185.
[17] L. Hoff, P.C. Sontum, J.M. Hovem, Oscillations of polymeric microbubbles: Effect of the encapsulating shell, J. Acoust. Soc. Am. 107 (4) (2000) 2272–2280.
[18] J.S. Allen, D.J. May, K.W. Ferrara, Dynamics of therapeutic ultrasound contrast agents, Ultrasound Med. Biol. 28 (6) (2002) 805–816.
[19] P. Marmottant, S. van der Meer, M. Emmer, M. Versluis, N. de Jong, S. Hilgenfeldt, D. Lohse, A model for large amplitude oscillations of coated bubbles accounting for buckling and rupture, J. Acoust. Soc. Am. 118 (6) (2005) 3499–3505.
[20] S. Paul, A. Katiyar, K. Sarkar, D. Chatterjee, W.T. Shi, F. Forsberg, Material characterization of the encapsulation of an ultrasound contrast microbubble and its subharmonic response: Strain-softening interfacial elasticity model, J. Acoust. Soc. Am. 127 (6) (2010) 3846–3857.
[21] K. Yasui, J. Lee, T. Tuziuti, A. Towata, T. Kozuka, Y. Iida, Influence of the bubble-bubble interaction on destruction of encapsulated microbubbles under ultrasound, J. Acoust. Soc. Am. 126 (3) (2009) 973–982.
[22] M. Guédra, C. Cornu, C. Inserra, A derivation of the stable cavitation threshold accounting for bubble-bubble interactions, Ultrason. Sonochem. 38 (2017) 168–173.
[23] Y. Ye, Y. Liang, C. Dong, Y. Xu, Z. Zhang, Treating the phase change of cavitation as the source of vapor inside bubbles, Mod. Phys. Lett. B 35 (05) (2021) 2150093, https://doi.org/10.1142/S0217984921500937.
[24] S.-T. Ding, B. Luo, G. Li, A volume of fluid based method for vapor-liquid phase change simulation with numerical oscillation suppression, Int. J. Heat Mass Transf. 110 (2017) 348–359.
[25] M. Rahimi, S. Movahedirad, S. Shahhosseini, CFD study of the flow pattern in an ultrasonic horn reactor: Introducing a realistic vibrating boundary condition, Ultrason. Sonochem. 35 (2017) 359–374.
[26] G.S.B. Lebon, I. Tzanakis, G. Djambazov, K. Pericleous, D.G. Eskin, Numerical modelling of ultrasonic waves in a bubbly Newtonian liquid using a high-order acoustic cavitation model, Ultrason. Sonochem. 37 (2017) 660–668.
[27] Y. Ye, C. Dong, Z. Zhang, Y. Liang, Modeling acoustic cavitation in homogeneous mixture framework, Int. J. Multiph. Flow 122 (2020) 103142, https://doi.org/10.1016/j.ijmultiphaseflow.2019.103142.
[28] Y. Ye, C. Dong, Z. Zhang, Y. Liang, Considering the diffusive effects of cavitation in a homogeneous mixture model, Processes 8 (6) (2020) 662, https://doi.org/10.3390/pr8060662.
[29] J.-M. Gorce, M. Arditi, M. Schneider, Influence of Bubble Size Distribution on the Echogenicity of Ultrasound Contrast Agents: A Study of SonoVue™, Invest. Radiol. 35 (11) (2000) 661–671.
[30] C.E. Brennen, Cavitation and Bubble Dynamics, Oxford University Press, 1995.
[31] J. Tu, J.E. Swalwell, D. Giraud, W. Cui, W. Chen, T.J. Matula, Microbubble sizing and shell characterization using flow cytometry, IEEE Transactions on Ultrasonics Ferroelectrics & Frequency Control 58 (5) (2011) 955–963.
[32] K. Ando, T. Colonius, C.E. Brennen, Numerical simulation of shock propagation in a polydisperse bubbly liquid, Int. J. Multiph. Flow 37 (6) (2011) 596–608.
[33] E. Lauer, X.Y. Hu, S. Hickel, N.A. Adams, Numerical modelling and investigation of symmetric and asymmetric cavitation bubble dynamics, Comput. Fluids 69 (2012) 1–19.
[34] F. Li, J. Cai, X. Huai, B. Liu, Interaction mechanism of double bubbles in hydrodynamic cavitation, J. Therm. Sci. 22 (3) (2013) 242–249.